Adsorption of fluoride on a chitosan-based magnetic nanocomposite: equilibrium and kinetics studies

Abdolreza Abri, Mahmood Tajbakhsh and Ali Sadeghi

ABSTRACT

A new derivative of chitosan functionalized with chloroacyl chloride and 2-(2-aminoethylamino) ethanol was synthesized for the preparation of a magnetic nanocomposite containing Fe_3O_4@TiO_2 nanoparticles. Characterizations were done by Fourier transform infrared spectroscopy (FT-IR), X-ray diffraction (XRD), scanning electron microscopy (SEM), thermogravimetric analysis (TGA), and vibrating sample magnetometer (VSM). The nanocomposite was examined for the defluoridation of water, and the effect of contact time, pH, initial fluoride ion concentration, and adsorbent dosage were investigated. The Langmuir model showed the best agreement with the experimental data. The maximum adsorption capacity for the fluoride removal from aqueous solutions was 15.385 mg/g at 318 K and pH = 5.0. The adsorption mechanism matches the pseudo-second-order kinetic model with a rate constant (k_2) of 0.68 g/mg·min. The thermodynamics study of the nature of adsorption showed that ΔH and ΔS were 13.767 kJ/mol and 0.066 kJ/mol·K respectively. A mechanism for the fluoride sorption was proposed by considering the electrostatic and hydrogen bonding interactions.

Key words | adsorption, chitosan magnetic nanocomposite, fluoride, isotherm, kinetics

Abdolreza Abri
Ali Sadeghi
Chemistry Department,
Azarbaijan Shahid Madani University,
53714-161 Tabriz,
Iran

Mahmood Tajbakhsh (corresponding author)
Faculty of Chemistry,
University of Mazandaran,
Babolsar 47415,
Iran
E-mail: *mahmood.tajbakhsh32@gmail.com*

INTRODUCTION

Fluoride compounds are used for many purposes in industry including fertilizers, refining metals, ceramic production, etc. The fluoride-containing waste may mix with serviceable water leading to environmental pollution. The fluoride mineral, found in natural water systems, can enter our body through drinking water. According to the report of the World Health Organization (WHO), the maximum acceptable concentration of fluoride is 1.5 mg/L (Yao *et al.* 2009). Therefore, it is essential to maintain fluoride concentration at less than 1.5 mg/L in drinking water. Some methods used for removing the excess fluoride from drinking water include ion exchange, membrane processes, electrolysis, reverse osmosis, nanofiltration and adsorption (Nemade *et al.* 2002; Tor 2007; Liu *et al.* 2013). The adsorption method is among the most effective removal processes, because of its high efficiency, low cost and environmentally friendly procedure. Various researchers have used different adsorbents such as zeolite (Cai *et al.* 2015), protonated chitosan (Huang *et al.* 2012), and biocomposites (Mahdavinia & Mosallanezhad 2016) for the defluoridation of water. However, some of these adsorbents show low adsorption capacity at low fluoride concentration, and some others are expensive. A green technique for toxic ion removal is biosorption. Special attention has been paid to bio-adsorbents due to their easy availability and properties of being biocompatible and biodegradable (Bektaş & Kara 2004). Cellulose, chitin and chitosan are cheap and easily available biopolymers used as bio-adsorbents. Chitosan is an excellent bio-adsorbent for the removal of heavy metals and fluoride from industrial wastewater (Haider & Park 2009). However,

doi: 10.2166/ws.2018.050

some modification of chitosan has been applied to improve its adsorption capacity for the removal of cations and anions. In addition, reusability of the adsorbents is very important especially when the particle size is in nanoscale, which may reduce the contact time in each cycle. The recovery of the magnetic adsorbents from the purified water could be facilitated using an external magnetic field in the water treatment application.

The present study focuses on the synthesis and characterization of a modified magnetic chitosan nanocomposite for fluoride removal. The performance of this nanocomposite was assessed by kinetics and thermodynamics of adsorption. Parameters such as contact time, pH and temperature were considered in this study. The best model for the sorption system was obtained by examining the equilibrium sorption data with various isotherms. Also, the thermodynamic parameters were determined to find the nature of fluoride sorption.

MATERIALS AND METHODS

Chemical reagents

Ferric chloride ($FeCl_3{\cdot}6H_2O$), ferrous chloride ($FeCl_2{\cdot}4H_2O$), ammonium hydroxide (25 wt%), hydrochloric acid, sodium hydroxide, sodium chloride and methanol were all obtained from Merck Company. Chitosan (CS) (deacetylation degree 85%), chloroacyl chloride (CAC), 2-(2-aminoethylamino) ethanol (AEAE), N-methylpyrrolidone (NMP), N,N-dimethylformamide (DMF), titanium(IV) oxide, acetone and diethyl ether were purchased from Sigma–Aldrich Company.

Preparation of Fe_3O_4@TiO_2

The magnetite nanoparticles were prepared using the conventional co-precipitation method with some modifications (Nabid *et al.* 2013). Typically, $FeCl_3{\cdot}6H_2O$ (2 g, 7.32 mmol) and $FeCl_2{\cdot}4H_2O$ (0.73 g, 2.70 mmol), dissolved in deionized water (40 mL) containing TiO_2 (1 g, 12.53 mmol) was stirred at 85 °C under nitrogen gas. NH_3, H_2O (25%, 3 mL) was then added slowly to the reaction medium and stirred for 20 min. The color of the solution changed to black immediately and the composite was removed by an external magnet, and washed with deionized water ($2 \times 1{,}000$ mL) and sodium chloride solution (2×20 mL). The black composite was dried at 50 °C in vacuum for 6 hours.

Preparation of modified chitosan composite

An amount of 1 g of chitosan was dissolved in NMP (45 mL) under argon and cooled to 0 °C. Chloroacyl chloride (CAC), dissolved in NMP (7 mL), was then added to the above solution. The reaction mixture was stirred at 0 °C for 15 min and then at ambient temperature for 3 h. After addition of diethyl ether, the resulting polymer was washed with methanol and dried at 50 °C in vacuum. Then, 0.5 g of this polymer was dissolved in dry DMF (20 mL) and stirred at 80 °C for 3 h, followed by the dropwise addition of 1 mL of 2-(2-aminoethylamino) ethanol and stirring for 24 h. Finally, 0.1 g of Fe_3O_4@TiO_2 was added and the mixture was stirred at 80 °C for 72 h. The black precipitate was separated by an external magnet and washed with ethanol and acetone. The resulting Fe_3O_4@TiO_2-CACS-AEAE nanocomposite was dried at 50 °C under vacuum for 6 h (Holappa *et al.* 2005).

Adsorption experiments

The adsorption experiments were carried out by mixing a certain amount of dry Fe_3O_4@TiO_2-CACS-AEAE, as nanoadsorbent, with sodium fluoride solution (40 mL, 2 ppm) at the desired pH. The pH was adjusted with 0.1 M HCl or 0.1 M NaOH. The mixture was shaken (SK-O330-Pro/SK-L330-Pro Dragon) with a speed of 300 rpm at room temperature. The fluoride concentrations in the solutions were determined at various time-intervals. The effect of contact time, pH, and adsorbent dosage was investigated on the defluoridation. Different initial fluoride concentrations (2–10 mg/L) were tested at pH = 5 and temperatures of 298, 308 and 318 K. A DR5000 UV-VIS spectrophotometer was used to measure the fluoride ion concentration. The adsorption percentage (S%) was calculated as in Equation (1):

$$S\% = \left(\frac{C_i - C_e}{C_i}\right) \times 100 \quad (1)$$

where C_i and C_e are the initial and final fluoride concentration (mg/L) before and after sorption, respectively. The adsorption capacity q_e (mg/g), was calculated as in Equation (2):

$$q_e = \left(\frac{C_i - C_e}{m}\right) \times V \quad (2)$$

where m (g) is the mass of nano-adsorbent and V (L) is the volume of the fluoride solution. All experiments were conducted in triplicate.

Characterization method

Fourier transform infrared spectroscopy (FT-IR) was taken on a Bruker Tensor 27 Spectrometer (Bruker, Karlsruhe, Germany). X-ray diffraction (XRD, Shibuya-ku, Japan) was recorded at room temperature on a RigakuD/Max-2550 powder diffractometer with a scanning rate of 5°/min, in the 2Θ range of 10–70. The surface morphology was examined by a scanning electron microscope (SEM) (Hitachi S4160 model) fitted with an energy dispersive X-ray analyzer (EDAX). Thermogravimetric analysis of nanoadsorbents was investigated using the LENSES STAPT-1000 calorimeter (Germany) by scanning up to 700 °C with a heating rate of 10 °C/min. The magnetization was determined by a vibrating sample magnetometer (VSM) (Daghigh Kavir Corporation, Iran) in an external field up to15 kOe at room temperature.

RESULTS AND DISCUSSION

Characterization of the sorbent

FT-IR spectra

The FT-IR spectra of Fe_3O_4@TiO_2, chitosan (CS), chitosan chloroacyl chloride (CACS), chitosan chloroacyl chloride-2-(2-aminoethylamino) ethanol (CACS-AEAE), and Fe_3O_4@TiO_2-CACS-AEAE before and after fluoride sorption are shown in Figure 1. The characteristic band of Fe_3O_4 and TiO_2 nanoparticles at 500–600 cm^{-1} are assigned to Fe-O and Ti-O bending vibrations (Galeotti *et al.* 2011). The peak at

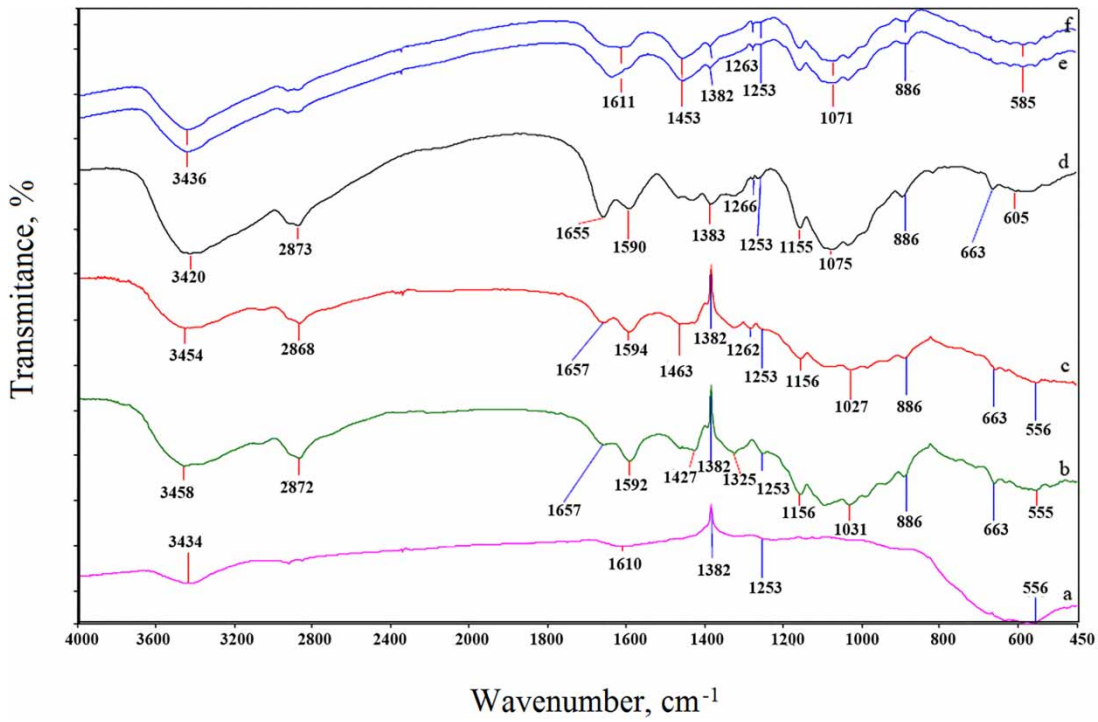

Figure 1 | FT-IR spectra of (a) Fe_3O_4@TiO_2, (b) chitosan, (c) chitosan chloroacyl chloride, (d) chitosan chloroacyl chloride-2-(2-aminoethylamino)ethanol, (e) nanocomposite, (f) nanocomposite after fluoride sorption.

3,434 cm^{-1} confirms the existence of OH on the surface of the Fe_3O_4 (Figure 1(a)). The spectrum of chitosan (Figure 1(b)) exhibits a broad signal at 3,458 cm^{-1} assigned to overlapped NH and OH stretching vibrations. The C = O stretching (amide I) peak near 1,655 cm^{-1} and the NH bending near 1,590 cm^{-1} are observed only in the spectrum of chitosan (Nunthanid *et al.* 2001). The spectrum of chitosan chloroacyl chloride (Figure 1(c)) displays vibration peaks at 3,100–3,600, 2,830–2,980, 1,680, 1,530, 1,262, and 1,150–950 cm^{-1} attributed to (O-H,NH), (C-H, pyranose), (amide I, N-chloroacyl), (amide II, N-chloroacyl), (CH_2Cl), and (C-O, pyranose) vibrations, respectively (Galeotti *et al.* 2011). In Figure 1(d), the bands at 3,400 and 1,655 cm^{-1} correspond to N-H and C = O stretching vibrations, respectively. The C-H stretching and OH bending vibrations are observed at 2,800–3,000 cm^{-1} and 1,400–1,450 cm^{-1}, respectively. Figure 1(e) and 1(f) represent the spectra of the composite before and after fluoride adsorption. Figure 1(e) shows all the expected vibration bands of its constituents, confirming their contribution in the final composite. The spectrum of the composite after fluoride adsorption (Figure 1(f)) is similar to that of the composite before adsorption with a slight broadening of vibrations at 3,436, 1,655 and 1,590 cm^{-1}, which are characteristics of NH and OH, and C = O stretching and NH bending vibrations, respectively (Nunthanid *et al.* 2001). This could be due to the hydrogen bonding between adsorbed fluoride ions with the composite surface (Viswanathan *et al.* 2009a). The similarity of the two spectra (Figure 1(e) and 1(f)) indicates that the structure of the nanocomposite is not changed after adsorption.

XRD

Figure 2 shows the XRD patterns of Fe_3O_4@TiO_2, chitosan chloroacyl chloride-2-(2-aminoethylamino) ethanol (CACS-AEAE), and Fe_3O_4@TiO_2-CACS-AEAE before and after fluoride adsorption. In Figure 2(a), the characteristic peaks at 2Θ = 24–26, 37–39, 48, 54, 55 and 69–71 are attributed to the tetragonal crystal planes of anatase TiO_2. Moreover, the peaks at 2Θ = 30, 35.3, 43–44 and 62–64 are associated with the crystal planes of Fe_3O_4. In Figure 2(b), the characteristic peak of

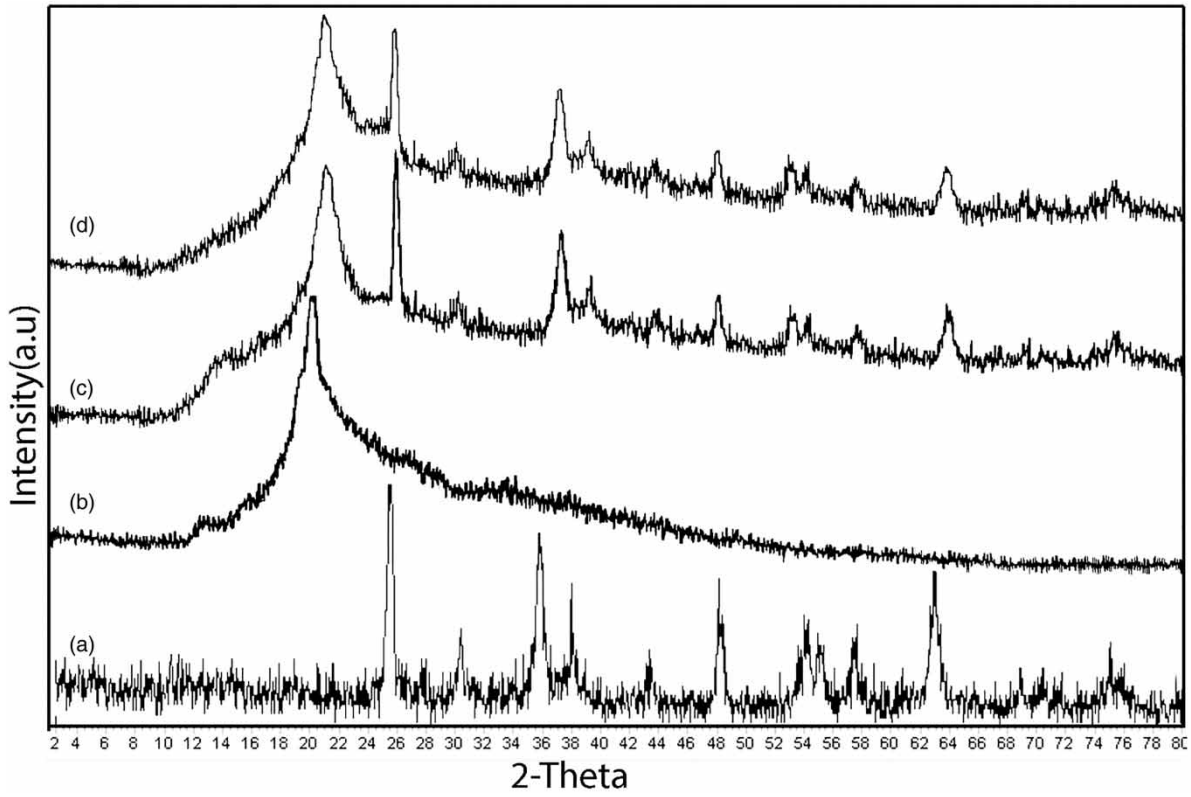

Figure 2 | XRD patterns of (a) Fe_3O_4@TiO_2, (b) CACS-AEAE, (c) nanocomposite and (d) nanocomposite after fluoride sorption.

modified chitosan is observed at $2\Theta = 20–22$, representing the amorphous structure of chitosan. In the XRD patterns of the nanocomposite before (Figure 2(c)) and after (Figure 2(d)) fluoride adsorption, all the characteristic peaks of chitosan, Fe_3O_4 and TiO_2 are observed, which could confirm the successful functionalization of the parent chitosan during nanocomposite preparation. However, as shown in Figure 2(d), after fluoride adsorption no marked changes are observed in the XRD patterns, indicating that there are no obvious changes in crystal structure after adsorption of fluoride (Figure 2(d)).

SEM and EDAX analyses

The SEM images together with the EDAX spectra, shown in Figure 3, prove fluoride adsorption on the nanocomposite. Many cavities before the sorption are no longer present on the nanocomposite after sorption, which can be indicative of fluoride adsorption. Also, from the EDAX spectra in Figure 3(c) and 3(d) the presence of fluoride on the nanocomposite after adsorption is clear.

Thermal properties of nanoadsorbent

The thermogravimetric analysis (TGA) of chitosan chloroacyl chloride, 2-(2-aminoethylamino) ethanol (CACS-AEAE) and Fe_3O_4@TiO_2-CACS-AEAE nanocomposite is presented in Figure 4. Curves show a weight loss of 5–8% at temperatures below 200 °C, which is related to dehydration of surface water. The weight loss of 30–40% in the second step at 280–350 °C is due to the structural degradation of the samples. The weight losses of 17% for the modified chitosan and 12% for the nanocomposite at 350–800 °C are because of the

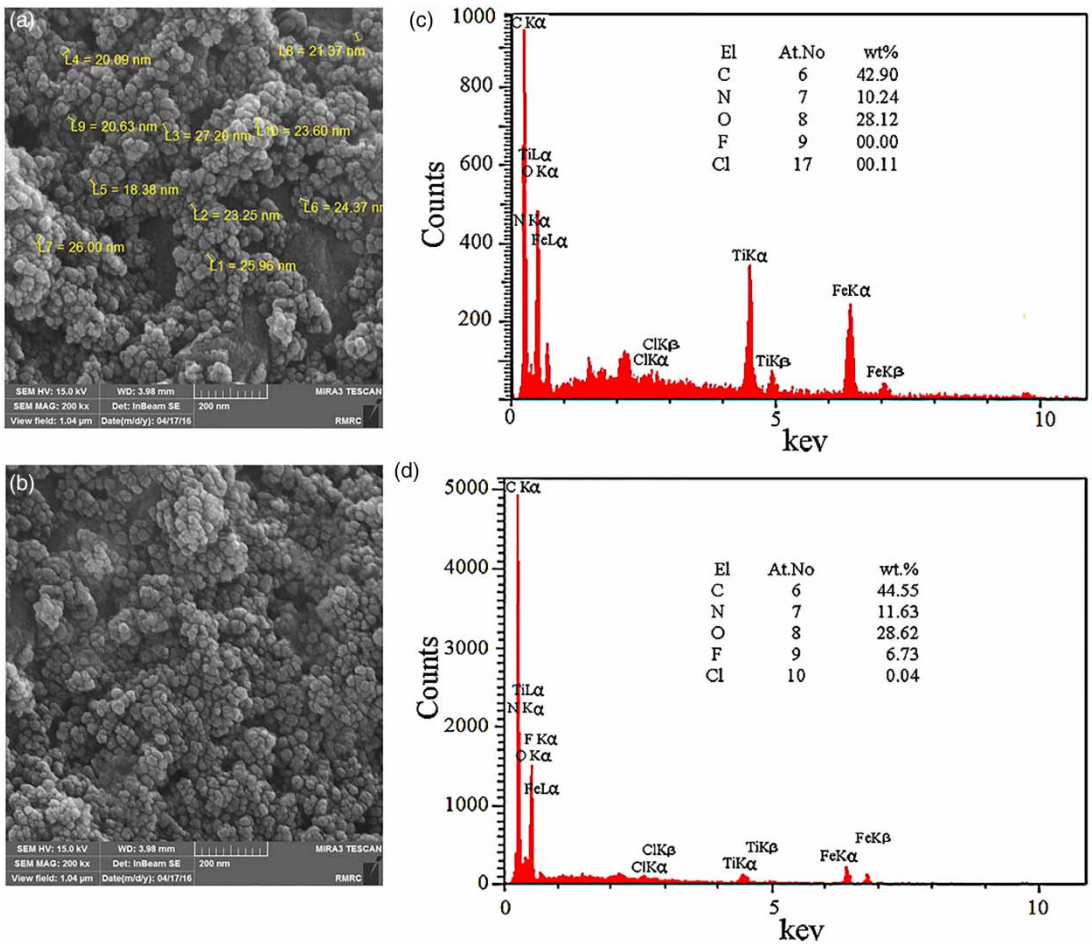

Figure 3 | SEM micrographs of (a) Fe_3O_4@TiO_2-CACS-AEAE, (b) Fe_3O_4@TiO_2-CACS-AEAE after fluoride adsorption along with the EDAX spectra of (c) Fe_3O_4@TiO_2-CACS-AEAE and (d) Fe_3O_4@TiO_2-CACS-AEAE after fluoride adsorption.

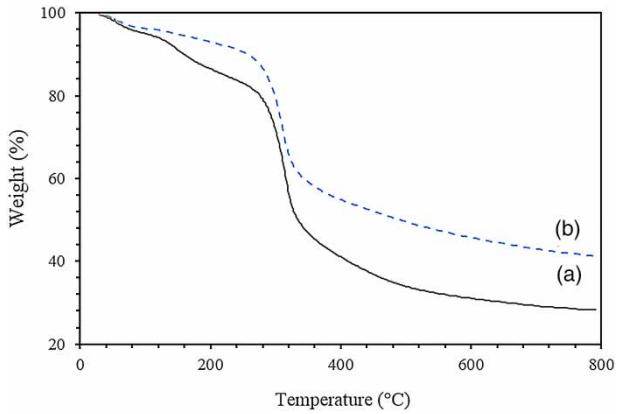

Figure 4 | TGA curves of (a) chitosan chloroacyl chloride-2-(2-aminoethylamino)ethanol (CACS-AEAE) and (b) Fe_3O_4@TiO_2-CACS-AEAE nanocomposite.

pyrolysis of the remaining materials to carbon residue resulting in the char yield of 28% and 48% for the modified chitosan and nanocomposite, respectively. These results show a higher thermal stability for the synthesized nanocomposite.

Magnetic properties

Magnetic hysteresis curves for the synthesized Fe_3O_4@TiO_2 nanoparticles and nanocomposite are displayed in Figure 5. Both samples are superparamagnetic because both remanence (M_r) and coercivity (H_c) are near zero. The Fe_3O_4@TiO_2-CACS-AEAE shows a smaller H_c and M_r compared with bare Fe_3O_4@TiO_2. This could be due to the presence of CACS-AEAE on the surface of the Fe_3O_4@TiO_2 which can reduce the magnetic properties.

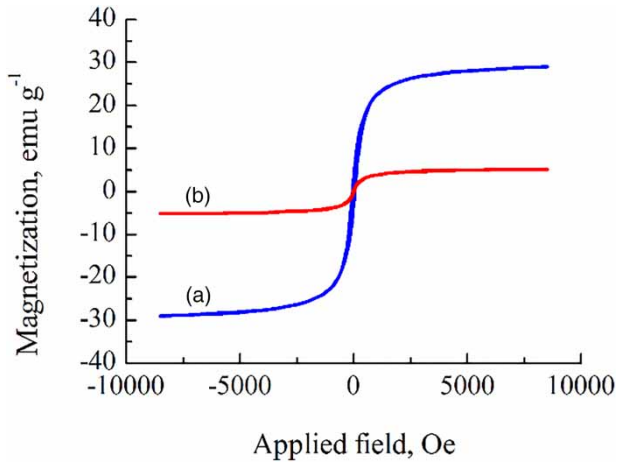

Figure 5 | VSM magnetization curves of (a) Fe_3O_4@TiO_2 nanoparticles and (b) Fe_3O_4@TiO_2-CACS-AEAE nanocomposite.

Effect of pH on the removal of fluoride

The effect of pH is associated with the solution chemistry and the ionization state of the sorbent functional groups. The adsorption experiments were carried out at pHs 3, 5, 7, 9 and 11. The effect of pH on the removal percentage is depicted in Figure 1S (supplementary data, available with the online version of this paper). As can be seen, increasing pH from 3 to 5 leads to an increase of fluoride adsorption from 58% to 92%. However, above pH = 5 the fluoride adsorption decreases. This observation indicates that at lower pH values the nanocomposite surface possesses more positive charges resulting in the higher adsorption of fluoride ions. At higher pH, the removal percentage decreases due to the repulsion between the negative hydroxide ions on the surface and fluoride ions. Therefore, pH = 5 was considered as the optimal pH for *further* studies. To gain more insight about the pH effect on the adsorption mechanism, the pH of zero point charge, pH_{zpc}, of the surface was determined by the drift method (Newcombe *et al.* 1993) to be 6 (Figure 2S, available online). This means that at pH values lower and higher than pH_{zpc} the surface of the composite has positive and negative charges, respectively. Therefore, electrostatic interactions are stronger between the nanocomposite surface and fluoride ions at $pH < pH_{zpc}$, in agreement with the results obtained for the optimal pH of 5.

Effect of adsorbent dosage on fluoride adsorption

The adsorbent dosage effect on fluoride removal was investigated for different amounts of the adsorbent (5 to 40 mg) in 50 mL of fluoride solution at room temperature and contact time of 120 min. Fluoride ion adsorption increases with increasing the amount of nanocomposite (Figure 3S, available online). However, the efficiency of fluoride removal does not change significantly for an adsorbent dosage of more than 20 mg, which might be due to the fewer available binding sites for the fluoride ions on the adsorbent surface.

Effect of contact time

Contact time in the range of 5–120 min was examined in aqueous solution. An adsorption efficiency of 58% and an

adsorption capacity of 3.3 mg/g were achieved after 5 min for the initial fluoride concentration 2 mg/L (Figure 4S, available online). The adsorption increased to 91% after 30 min and did not change up to 120 min. Therefore, we consider the contact time of 30 min, which has the maximum fluoride adsorption, for further studies.

Effect of the initial fluoride concentration

The effect of the initial fluoride concentration on adsorption is shown in Figure 5S (available online). The maximum adsorption was found for the initial fluoride concentration of 2 mg/L, and further increasing the initial concentration lead to lower fluoride removal. This may be due to the full coverage of active surface sites at high adsorbate concentration, therefore at higher concentrations, no active surface is available, which results in the decreasing percentage of fluoride removal.

The adsorption equilibrium isotherm

Three commonly used isotherms, Langmuir, Freundlich and Temkin, were adopted to evaluate the sorption capacity of the nanocomposite for fluoride removal from aqueous solution (Matouq *et al.* 2015). The Langmuir equation, which is reliable for monolayer adsorption onto a surface, is given by Equation (3):

$$\frac{C_e}{q_e} = \frac{1}{q_{mb}} + \left(\frac{1}{q_m}\right) C_e \tag{3}$$

where q_m is the maximum amount of the fluoride ion adsorbed (mg/g), b (L/mg) is the Langmuir constant, and q_e, is the amount of fluoride adsorbed per unit weight of the sorbent (mg/g). A linear plot of C_e/q_e against C_e is shown in Figure 6S(a), from the slope and intercept of which the values of q_m and b can be determined, respectively (Figure 6S is available online). According to Table 1, the increase in q_m values with respect to temperature shows that the fluoride sorption is an endothermic process. The correlation coefficient ($r > 0.99$) could indicate the applicability of the Langmuir isotherm for the sorption of fluoride ions in aqueous solution. In order to evaluate the feasibility of the isotherm, a dimensionless constant separation factor or equilibrium parameter is expressed as in Equation (4):

Table 1 | Adsorption isotherm parameters for the removal of fluoride by the synthesized nanocomposite

		Temperature (K)		
Isotherm mode	**Parameters**	**298**	**308**	**318**
Langmuir	q_m(mg/g)	14.620	14.641	15.385
	b(l/g)	1.834	1.876	2.097
	r	0.990	0.995	0.993
	sd	0.003	0.002	0.003
	X^2	0.015	0.011	0.008
	R_l	0.145	0.142	0.129
Freundlich	n	2.611	2.398	2.525
	k_f(mg/g)(l/g)$^{1/n}$	8.198	8.241	8.908
	r	0.848	0.957	0.973
	sd	0.065	0.019	0.023
	X^2	0.279	0.080	0.101
Temkin	k_T(l/g)	9.759	9.666	20.211
	B	9.261	9.048	9.455
	r	0.960	0.972	0.984
	sd	0.190	0.167	0.125
	X^2	0.781	0.670	0.538

$$R_l = \frac{1}{1 + bC_0} \tag{4}$$

where C_0 is the initial fluoride concentration (mg/L). R_l was less than 1 at the different temperatures studied (Table 1). This indicates favorable fluoride sorption conditions at the different temperatures (Gandhi *et al.* 2012).

The surface heterogeneity of the sorbent was studied using the Freundlich model as in Equation (5):

$$\log q_e = \log K_f + \left(\frac{1}{n}\right) \log C_e \tag{5}$$

where k_f is a measure of sorption capacity and $1/n$ is the sorption intensity. The values of n and k_f can be obtained from the slope and intercept of the linear plot of $\ln q_e$ vs $\ln C_e$ (Figure 6S(b)). These values for the studied magnetic nanocomposite are listed in Table 1. Values of n in the range of 1–10 confirm favorable conditions for sorption. Increasing k_f from 8.198 to 8.908 [(mg/g)(l/mg)$^{1/n}$] with increasing temperature confirms the endothermic nature of the process, in agreement with the Langmuir isotherm results.

The third isotherm used to fit the experimental data is the Temkin isotherm as in Equation (6):

$$q_e = B \ln A + B \ln C_e \quad (6)$$

The A (Temkin isotherm constant (l/g)) and B (RT/b_t, where b_t is the Temkin constant related to heat of sorption (J/mol), R is the universal gas constant (8.314 J/mol K) and T is absolute temperature (K)) were determined from the slope and intercept of the linear plot of q_e vs $\ln C_e$ (Figure 6S(c)) and are listed in Table 1. The applicability of this isotherm can be shown by the high r and the low sd values.

Chi-square analysis

The chi-square analysis was used to determine the appropriate isotherm. The mathematical equation for chi-square is shown as Equation (7):

$$X^2 = \sum \frac{(q_e - q_{e,m})^2}{q_{e,m}} \quad (7)$$

where $q_{e,m}$ is the equilibrium capacity (mg/g) determined from the model. X^2 is small if $q_{e,m}$ and q_e are close to each other, and therefore, the corresponding model can predict the adsorption process more reliably. Hence, it is necessary to analyze the studied dataset using the non-linear chi-square test to confirm the best-fit isotherm. Values of X^2 for the fluoride adsorption are presented in Table 1. X^2 related to the three studied models indicates the reliability of the models in the order of Langmuir>Freundlich>Temkin isotherms. The Langmuir isotherm, which is the best-fitting model, shows that the adsorption is mostly monolayer.

The adsorption kinetics

Two kinetic models were used to understand the adsorption mechanism. The pseudo-first-order and pseudo-second-order models were employed for the kinetic analysis of fluoride sorption on the magnetic nanocomposite. The pseudo-first-order equation is given as Equation (8):

$$\log(q_e - q_t) = \log q_e - \frac{k_1}{2.303} t \quad (8)$$

where q_t (mg/g) is the amount of fluoride on the surface of the nanocomposite at time t, and k_1 is the equilibrium rate constant (1/min). For the pseudo-second-order model the most popular linear form is:

$$\frac{t}{q_e} = \frac{1}{k_2 q_2^2} + \frac{t}{q_2} \quad (9)$$

where q_2 (mg/g) is the maximum adsorption capacity for the uptake and k_2 (1/min) is the rate constant of fluoride in the pseudo-second-order adsorption process; the initial adsorption rate is $k_2 q_2^2$ (mg/g min) (Yurdakoç *et al.* 2005). The plots of these two models are shown in Figure 7S (available online). The linearity of the plot, shown in Figure 7S(b), confirms the applicability of the pseudo-second-order kinetic equation for the adsorption of fluoride on the nanocomposite under optimal conditions. The values of q_e, k_1, k_2, q_2 and r for the adsorption of fluoride were obtained from the slopes and intercepts of the plots and are given in Table 2.

Determination of thermodynamic parameters

The values of thermodynamic parameters are reported in Table 3. The standard free energy change was calculated as in Equation (10):

$$\Delta G^\circ = -RT \ln K_0 \quad (10)$$

where ΔG° is the standard free energy of sorption (kJ/mol), T is the temperature (K), R is the universal gas constant (8.314 J/mol·K), and K_o is the sorption equilibrium coefficient. The K_o value was obtained from the slope of the plot of $\ln(q_e/C_e)$ against C_e at different temperatures by

Table 2 | Comparison between the parameters of pseudo-first-order and pseudo-second-order kinetic models for the adsorption of fluoride on the nanocomposite

		Temperature (K)		
Kinetic models	**Parameters**	**298**	**308**	**318**
Pseudo-first-order	q_1(mg/g)	4.524	4.505	4.739
	k_1 (1/min)	1.588	2.108	0.145
	r	0.826	0.798	0.960
	sd	0.080	0.110	0.072
Pseudo-second-order	q_2(mg/g)	4.854	4.878	5.025
	k_2 (g mg/min)	0.687	0.723	0.685
	r	0.990	0.992	0.996
	sd	0.010	0.009	0.006

Table 3 | Thermodynamic parameters for the adsorption of fluoride on the nanocomposite

Temperature (K)	ΔG° (kJ/mol)	ΔH° (kJ/mol)	ΔS° (kJ/mol·K)
298	−5.946	13.767	0.066
308	−6.404		
318	−7.141		

extrapolating to zero C_e according to the Khan and Singh method (Khan & Singh 1987). The sorption equilibrium coefficient may be explained in terms of ΔH° and ΔS° as a function of temperature as in Equation (11):

$$\ln K_0 = \frac{\Delta S^\circ}{R} - \frac{\Delta H^\circ}{RT} \tag{11}$$

where ΔH° is the standard enthalpy change (kJ/mol) and ΔS° is the standard entropy change (kJ/mol·K). The values of ΔH° and ΔS° can be obtained from the respective slope and intercept of the plot of $\ln K_o$ against $1/T$. As can be seen in Table 3, the negative values of ΔG° confirm the spontaneous nature of

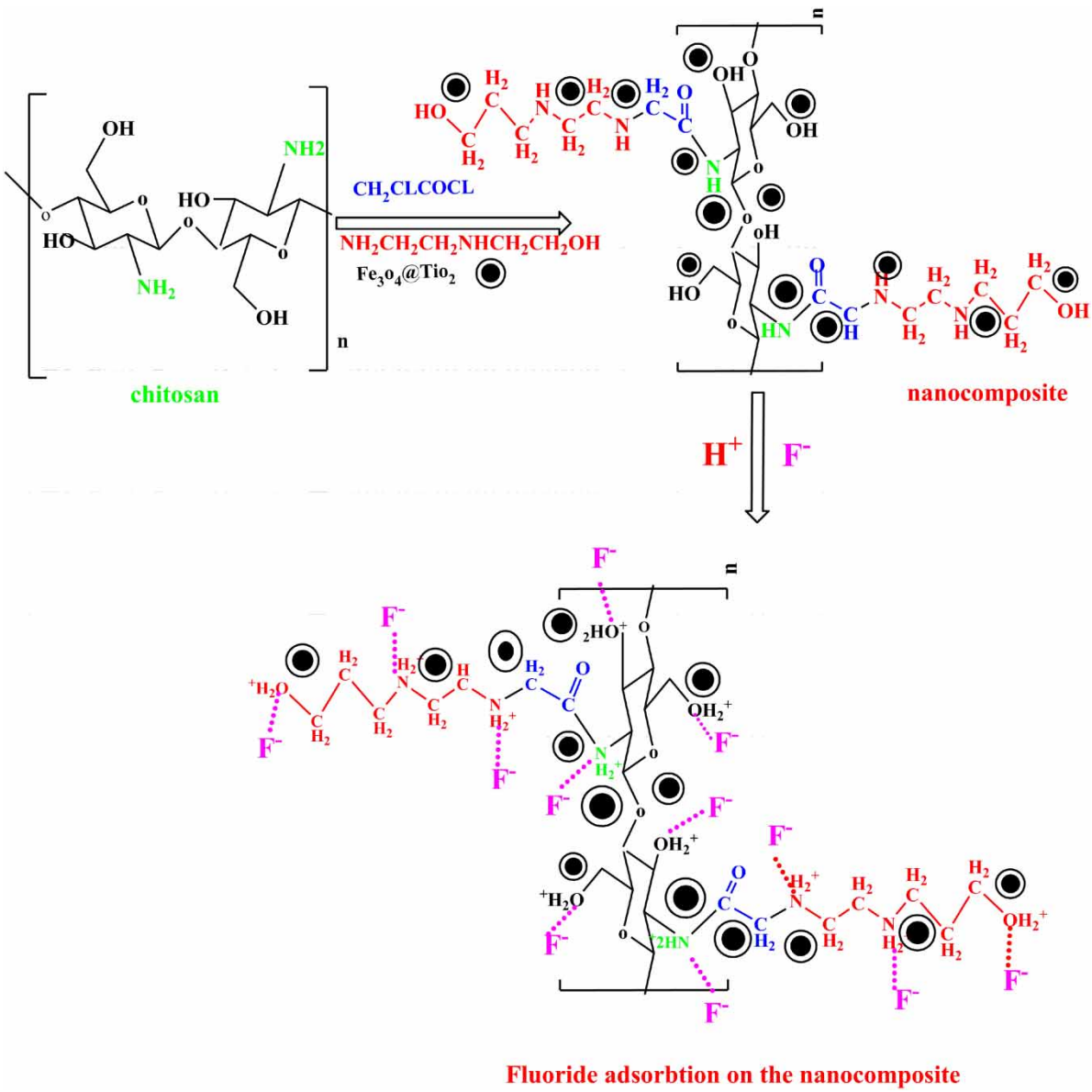

Figure 6 | Proposed mechanism of fluoride removal by the nanocomposite.

fluoride sorption. Furthermore, negatively higher values of ΔG° are seen at higher temperatures suggesting that the adsorption becomes more favorable at higher temperatures. The values of ΔH° are positive indicating that the sorption process is endothermic in agreement with the discussion on the above-mentioned studied isotherms. The positive value of ΔS° indicates the possibility of randomness at the solid/liquid interface during fluoride sorption.

Mechanism of fluoride removal by the nanocomposite

Figure 6 shows the proposed mechanism for fluoride removal by the nanocomposite (Prabhu *et al.* 2014). The positively charged species on the surface of the nanocomposite, NH_3^+ and OH_2^+, attract negatively charged fluoride ions through electrostatic attractions. The presence of more functional groups ($-NH_3^+$ and OH_2^+) results in the high adsorption capacity of the nanocomposite for fluoride removal. Furthermore, the synthesized nanocomposite may be considered as hard acid as it possesses H^+ ions, and therefore, it prefers to bind with hard bases, such as fluoride with high electronegativity and low polarizability (Pearson 1963). Therefore, the high removal capacity of fluoride can be due to the presence of NH_3^+, OH_2^+, Fe^{2+} and Fe^{3+} species in the studied nanocomposite. To show the effective ability of our nanocomposite, the fluoride adsorption capacity of some common sorbents available in the literature is presented in Table 4.

Regeneration and reusability of the nanocomposite

The regeneration and reusability studies of the magnetic nanocomposite were performed by the sorption, separation, washing, regeneration and reuse cycle five times using 20 ml of NaOH solution with concentrations of 0.05, 0.1, and 0.5 M. A maximum desorption of 90.15% was observed by 0.1 M NaOH solution. Therefore, 0.1 M NaOH solution is a suitable eluent for the regeneration of the magnetic nanocomposite. As shown in Figure 7, the fluoride sorption efficiencies of the nanocomposite from five cycles were 87.23%, 85.24%, 80.26%, 78.58% and 74.64%, respectively. These efficiencies suggest that the magnetic nanocomposite is regenerable and can be effectively used for multiple cycles (Ekka *et al.* 2017).

Table 4 | Fluoride adsorption capacity of some reported sorbents

Adsorbent	Adsorption capacity (mg/g)	Reference
Carboxylated chitosan beads	1.385	Viswanathan *et al.* (2009b)
Nanohydroxyapatite/chitosan composite	1.560	Sundaram *et al.* (2008)
Cerium(III)-loaded silica gel/chitosan biocomposite	4.821	Muthu Prabhu & Meenakshi (2014)
Mixed rare earths modified chitosan	3.72	Liang *et al.* (2013)
Chitosan supported mixed metal oxides beads	4.97	Prabhu & Meenakshi (2014)
Chitosan supported mixed metal oxides	4.58	Prabhu *et al.* (2014)
Our modified chitosan magnetic nanocomposite	4.635	Present study

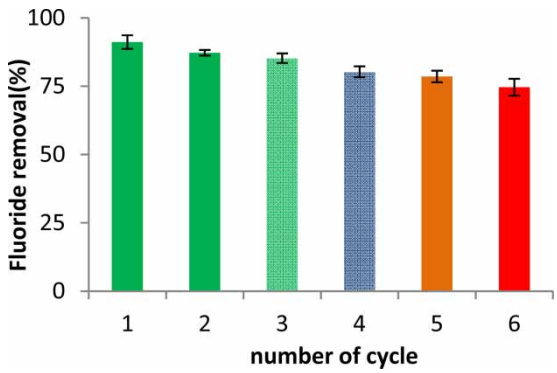

Figure 7 | Percentage of fluoride removal by the nanocomposite in different cycles.

CONCLUSIONS

The novel magnetic chitosan-based nanocomposite functionalized with chloroacyl chloride and 2-(2-aminoethylamino) ethanol showed a good ability for the removal of fluoride. Factors such as contact time, pH, co-existing anions, initial fluoride concentration and temperature affected the fluoride adsorption. The maximum removal of fluoride by the magnetic nanocomposite was determined at pH 5.0. The thermodynamic parameters indicated that the sorption of fluoride on the

magnetic nanocomposite was a spontaneous process. This adsorption process was best fitted with the Langmuir isotherm, which shows that the adsorption is mostly monolayer. The kinetics study confirmed that the adsorption mechanism was based on the pseudo-second-order kinetic model. Also, the fluoride adsorption was controlled by electrostatic attraction via hydrogen bonding. The results of this study showed that the synthesized nanocomposite can effectively decrease the fluoride level even in the presence of other anions, and therefore, it can be used as an effective and favorable defluoridating agent.

REFERENCES

Bektaş, N. & Kara, S. 2004 Removal of lead from aqueous solutions by natural clinoptilolite: equilibrium and kinetic studies. *Separation and Purification Technology* **39** (3), 189–200.

Cai, Q., Turner, B. D., Sheng, D. & Sloan, S. 2015 The kinetics of fluoride sorption by zeolite: effects of cadmium, barium and manganese. *Journal of Contaminant Hydrology* **177–178**, 136–147.

Ekka, B., Dhaka, R. S., Patel, R. K. & Dash, P. 2017 Fluoride removal in waters using ionic liquid-functionalized alumina as a novel adsorbent. *Journal of Cleaner Production* **151**, 303–318.

Galeotti, F., Bertini, F., Scavia, G. & Bolognesi, A. 2011 A controlled approach to iron oxide nanoparticles functionalization for magnetic polymer brushes. *Journal of Colloid and Interface Science* **360** (2), 540–547.

Gandhi, M. R., Kousalya, G. N. & Meenakshi, S. 2012 Selective sorption of Fe(III) using modified forms of chitosan beads. *Journal of Applied Polymer Science* **124** (3), 1858–1865.

Haider, S. & Park, S.-Y. 2009 Preparation of the electrospun chitosan nanofibers and their applications to the adsorption of Cu(II) and Pb(II) ions from an aqueous solution. *Journal of Membrane Science* **328** (1–2), 90–96.

Holappa, J., Nevalainen, T., Soininen, P., Elomaa, M., Safin, R., Másson, M. & Järvinen, T. 2005 *N*-chloroacyl-6-*O*-triphenylmethylchitosans: useful intermediates for synthetic modifications of chitosan. *Biomacromolecules* **6** (2), 858–863.

Huang, R., Yang, B., Liu, Q. & Ding, K. 2012 Removal of fluoride ions from aqueous solutions using protonated cross-linked chitosan particles. *Journal of Fluorine Chemistry* **141**, 29–34.

Khan, A. A. & Singh, R. P. 1987 Adsorption thermodynamics of carbofuran on Sn (IV) arsenosilicate in H^+, Na^+ and Ca^{2+} forms. *Colloids and Surfaces* **24** (1), 33–42.

Liang, P., Zhang, Y., Wang, D., Xu, Y. & Luo, L. 2013 Preparation of mixed rare earths modified chitosan for fluoride adsorption. *Journal of Rare Earths* **31** (8), 817–822.

Liu, Q., Huang, R., Yang, B. & Liu, Y. 2013 Adsorption of fluoride from aqueous solution by enhanced chitosan/bentonite composite. *Water Science and Technology* **68** (9), 2074–2081.

Mahdavinia, G. R. & Mosallanezhad, A. 2016 Facile and green rout to prepare magnetic and chitosan-crosslinked κ-carrageenan bionanocomposites for removal of methylene blue. *Journal of Water Process Engineering* **10**, 143–155.

Matouq, M., Jildeh, N., Qtaishat, M., Hindiyeh, M. & Al Syouf, M. Q. 2015 The adsorption kinetics and modeling for heavy metals removal from wastewater by *Moringa* pods. *Journal of Environmental Chemical Engineering* **3** (2), 775–784.

Muthu Prabhu, S. & Meenakshi, S. 2014 Synthesis of metal ion loaded silica gel/chitosan biocomposite and its fluoride uptake studies from water. *Journal of Water Process Engineering* **3**, 144–150.

Nabid, M. R., Sedghi, R., Gholami, S., Oskooie, H. A. & Heravi, M. M. 2013 Preparation of new magnetic nanocatalysts based on TiO_2 and ZnO and their application in improved photocatalytic degradation of dye pollutant under visible light. *Photochemistry and Photobiology* **89** (1), 24–32.

Nemade, P. D., Vasudeva Rao, A. & Alappat, B. J. 2002 Removal of fluorides from water using low cost adsorbents. *Water Science and Technology: Water Supply* **2** (1), 311–317.

Newcombe, G., Hayes, R. & Drikas, M. 1993 Granular activated carbon: importance of surface properties in the adsorption of naturally occurring organics. *Colloids and Surfaces A: Physicochemical and Engineering Aspects* **78**, 65–71.

Nunthanid, J., Puttipipatkhachorn, S., Yamamoto, K. & Peck, G. E. 2001 Physical properties and molecular behavior of chitosan films. *Drug Development and Industrial Pharmacy* **27** (2), 143–157.

Pearson, R. G. 1963 Hard and soft acids and bases. *Journal of the American Chemical Society* **85** (22), 3533–3539.

Prabhu, S. M. & Meenakshi, S. 2014 Enriched fluoride sorption using chitosan supported mixed metal oxides beads: synthesis, characterization and mechanism. *Journal of Water Process Engineering* **2**, 96–104.

Prabhu, S. M., Viswanathan, N. & Meenakshi, S. 2014 Defluoridation of water using chitosan assisted ethylenediamine functionalized synthetic polymeric blends. *International Journal of Biological Macromolecules* **70**, 621–627.

Sundaram, C. S., Viswanathan, N. & Meenakshi, S. 2008 Uptake of fluoride by nano-hydroxyapatite/chitosan, a bioinorganic composite. *Bioresource Technology* **99** (17), 8226–8230.

Tor, A. 2007 Removal of fluoride from water using anion-exchange membrane under Donnan dialysis condition. *Journal of Hazardous Materials* **141** (3), 814–818.

Viswanathan, N., Sundaram, C. S. & Meenakshi, S. 2009a Development of multifunctional chitosan beads for fluoride removal. *Journal of Hazardous Materials* **167** (1–3), 325–331.

Viswanathan, N., Sundaram, C. S. & Meenakshi, S. 2009b Sorption behaviour of fluoride on carboxylated cross-linked chitosan beads. *Colloids and Surfaces B: Biointerfaces* **68** (1), 48–54.

Yao, R., Meng, F., Zhang, L., Ma, D. & Wang, M. 2009 Defluoridation of water using neodymium-modified chitosan. *Journal of Hazardous Materials* **165** (1–3), 454–460.

Yurdakoç, M., Seki, Y., Karahan, S. & Yurdakoç, K. 2005 Kinetic and thermodynamic studies of boron removal by Siral 5, Siral 40, and Siral 80. *Journal of Colloid and Interface Science* **286** (2), 440–446.

First received 11 July 2017; accepted in revised form 19 February 2018. Available online 5 March 2018